

# Evidence of Elevated X-Ray Absorption Before and During Major Flare Ejections in GRS 1915+105

Brian Punsly<sup>1</sup>, Jérôme Rodriguez<sup>2</sup> and Sergei A. Trushkin<sup>3</sup>

## ABSTRACT

We present time resolved X-ray spectroscopy of the microquasar GRS1915+105 with the MAXI observatory in order to study the accretion state just before and during the ejections associated with its major flares. Radio monitoring with the RATAN-600 radio telescope from 4.8 - 11.2 GHz has revealed two large steep spectrum major flares in the first eight months of 2013. Since, the RATAN receives one measurement per day, we cannot determine the jet forming time without more information. Fortunately, this is possible since a distinct X-ray light curve signature that occurs preceding and during major ejections has been determined in an earlier study. The X-ray luminosity spikes to very high levels in the hours before ejection then becomes variable (with a nearly equal X-ray luminosity when averaged over the duration of the ejection) during a brief 3 to 8 hour ejection process. By comparing this X-ray behavior to MAXI light curves, we can estimate the beginning and end of the ejection episode of the strong 2013 flares to within  $\sim 3$  hours. Using this estimate in conjunction with time resolved spectroscopy from the data in the MAXI archives allows us to deduce that the X-ray absorbing hydrogen column density increases significantly in the hours preceding the ejections and remains elevated during the ejections responsible for the major flares. This finding is consistent with an out-flowing wind or enhanced accretion at high latitudes.

*Subject headings:* Black hole physics — magnetohydrodynamics (MHD) — galaxies: jets—galaxies: active — accretion, accretion disks

---

<sup>1</sup>1415 Granvia Altamira, Palos Verdes Estates CA, USA 90274 and ICRANet, Piazza della Repubblica 10 Pescara 65100, Italy, brian.punsly1@verizon.net or brian.punsly@comdev-usa.com

<sup>2</sup>Laboratoire AIM, CEA/DSM-CNRS-Université Paris Diderot, IRFU SAp, F-91191 Gif-sur-Yvette, France.

<sup>3</sup>Special Astrophysical Observatory RAS, Nizhnij Arkhyz, 369167, Russia

## 1. Introduction

Astrophysical black holes reveal themselves to astronomers through their interaction with adjacent gas. There are two observed aspects to this phenomenon, the thermal glow from the viscously heated accreting gas and the bipolar ejection of plasma that can propagate very close to the speed of light. Both behaviors are seen in solar mass black holes (microquasars) in the Milky Way as well as supermassive black holes in active galactic nuclei (AGN). The relationship between the accretion and jet formation has been intensely studied (eg, Fender et al. (2004), but is still not well understood. Microquasars have a logistical advantage for astronomers since significant evolution of the system can happen on short time scales (ms to days). Thus, direct associations between accretion and outflow diagnostics can be discerned, in principal, within a human lifetime (Rodriguez et al. 2008; Miller-Jones et al. 2012). By contrast, AGN vary on the time scales of  $\sim 1 - 10^6$  years. Thus, the chance of gathering enough information to make statistically significant correlations between accretion and outflow observable quantities in a human lifetime is drastically diminished. Hence, the appeal of using microquasars as time compressed laboratories to study black hole and quasar physics. Substantial progress has been made in this regard for GRS 1915+105 which is well known for ejecting radio “blobs” out to large distances with apparent superluminal speeds (Mirabel and Rodriguez 1994; Fender et al. 1999; Dhawan et al. 2000). Punsly & Rodriguez (2013a, PR13 hereafter) analyzed large RXTE data sets and demonstrated that empirical relationships exist between the accretion states and major flare ejections. In particular, the X-ray luminosity is highly elevated in the last hours preceding major ejections and it is correlated with the power required to eject the discrete blobs of plasma at relativistic velocity. Secondly, the X-ray luminosity was found to be highly variable during major flare ejections (MFEs, hereafter), yet the time averaged X-ray luminosity during the ejection event is correlated with that just before the MFE and is of a similar (but perhaps a slightly lower) magnitude. However, the ejections are brief and occur at unpredictable times. Thus, all the relevant X-ray data are serendipitously gathered during wide field monitoring. Therefore, we have no pointed X-ray observations near or at the crucial instant of ejection and therefore no spectral data to constrain the accretion state. Ironically, in this circumstance, the rapid evolution of the microquasars impedes our understanding of the black hole accretion system. Fortunately, the MAXI observatory typically observes GRS 1915+105 every 1.5 hours and it has the ability to gather spectral data from 1 keV - 20 keV (Matsuoka et al. 2009). For very bright states (as occurs during major ejections), single epoch observations can provide a useful spectrum. For lower luminosity states, with slower evolution, one can bin multiple observations over a few hours to achieve sufficient signal to noise for a useful spectrum.

Being thusly motivated to understand the X-ray spectral state before and during major ejections, we have used the current monitoring program with RATAN-600 radio telescope to

find evidence of major ejections (i.e., large radio fluxes and a steep radio spectrum). Using a (limited) library of high temporal resolution X-ray light curves of major ejections from PR13, we estimate the time frame for flare ejection from the MAXI light curve. We downloaded the MAXI spectral data adjacent to this epoch and look for trends in the spectral fits and the raw number counts. Our findings, based on the two largest radio flares in the first eight months of 2013, are presented here.

## 2. Radio Monitoring

We were granted radio monitoring time on the RATAN-600 radio telescope at 4.8, 8.2 and 11.2 GHz for both the first and second half on 2013. These observations have been carried out in a current monitoring program of the microquasars with RATAN-600 (eg Trushkin et al. (2008)). The cryogenic cooled receivers and antenna were daily calibrated with secondary calibrators 3C286 and PKS1345+12. High luminosity, steep spectrum, radio flares originating from GRS 1915+105 have historically been associated with superluminal ejections (Rushton et al. 2010). Major flares begin as an optically thick flux increase that becomes optically thin at lower and lower frequency as they evolve over the next few hours. The temporal spacing of our monitoring program – one measurement per day – is far too large to estimate the time of the major ejection that is associated with the radio flare. From PR13 and Figure 1, ejection initiation and end times require temporal resolution 100 times finer, on the orders of 0.25 hours or less. However, strong flares are luminous for at least 1 day, so it is adequate for identifying major ejections (Rodriguez and Mirabel 1999; Miller-Jones et al. 2005). We define major flares as radio flares with a flux density  $S_\nu > 100$  mJy at frequency 4.8 GHz, with a steep spectral index,  $\alpha > 0.5$  ( $S_\nu \sim \nu^{-\alpha}$ ). We have identified 5 such major flares in the 8 first months of 2013.

The correlation of X-ray luminosity with flare energy and power shown in PR13 indicates that we should look at the strongest flares in order to get adequate statistics in our MAXI data. Of these five steep spectrum flares, two had  $S_\nu > 200$  mJy at 4.8 GHz. The first (hereafter Flare 1) was detected on MJD 56314.349 and the second (Flare 2) on MJD 56352.245. The observations adjacent to these flares are summarized in Table 1. In the following, we consider the MAXI spectral data for these flares. The other steep spectrum radio flares that were not suitable for spectral study with MAXI are discussed in the Appendix.

### 3. MAXI Observations of Major Flares

We downloaded the data from the MAXI pipeline around the times of the strong major radio flares listed in Table 1. We aim to accomplish two goals with these data. First is to estimate the dates that the major ejections occurred. Secondly, we implement time resolved MAXI spectroscopy to determine the evolution of the X-ray spectrum preceding and during major ejections.

#### 3.1. Estimating the Date of the Ejection Episode of Flare 2

According to Table 1, the detection on MJD 56352.245 indicates a strong flare that has evolved far past the launch point, since it is very steep spectrum. This flare is the primary topic of this study since it has the most complete MAXI spectral coverage. Without a timeline set by the beginning and end of the MFE episode, time resolved spectroscopy cannot be connected to a causal physical chain of events associated with the ejection process. Thus, establishing the date of the ejection episode is crucial to the following analysis.

##### 3.1.1. X-ray Diagnostics of Ejection

For sufficiently strong flares, the results of PR13 and Punsly and Rodriguez (2013b) can be used to define a clear X-ray light curve signature before and during major ejections. To this end, we utilize transcribed light curves from these references in Figure 1. In particular, the 4 light curves (based on the bolometric X-ray luminosity,  $L_{\text{bol}}$ ) for which we not only have X-ray luminosity estimates in the final hours preceding the ejection, but also at least two time separated luminosity estimates during the ejection proper. Inspection of the four light curves indicate the following behavior:

1. A large X-ray luminosity spike just before the MFE is launched.
2. During the ejection proper, the X-ray luminosity is highly variable.
3. There is always at least one dip in the X-ray luminosity during the MFE proper, well below the pre-launch value.
4. From Figure 1, PR 13 and Punsly and Rodriguez (2013b), the time averaged X-ray luminosity during launch is highly correlated with the luminosity preceding the launch with a similar (but perhaps slightly smaller) luminosity.

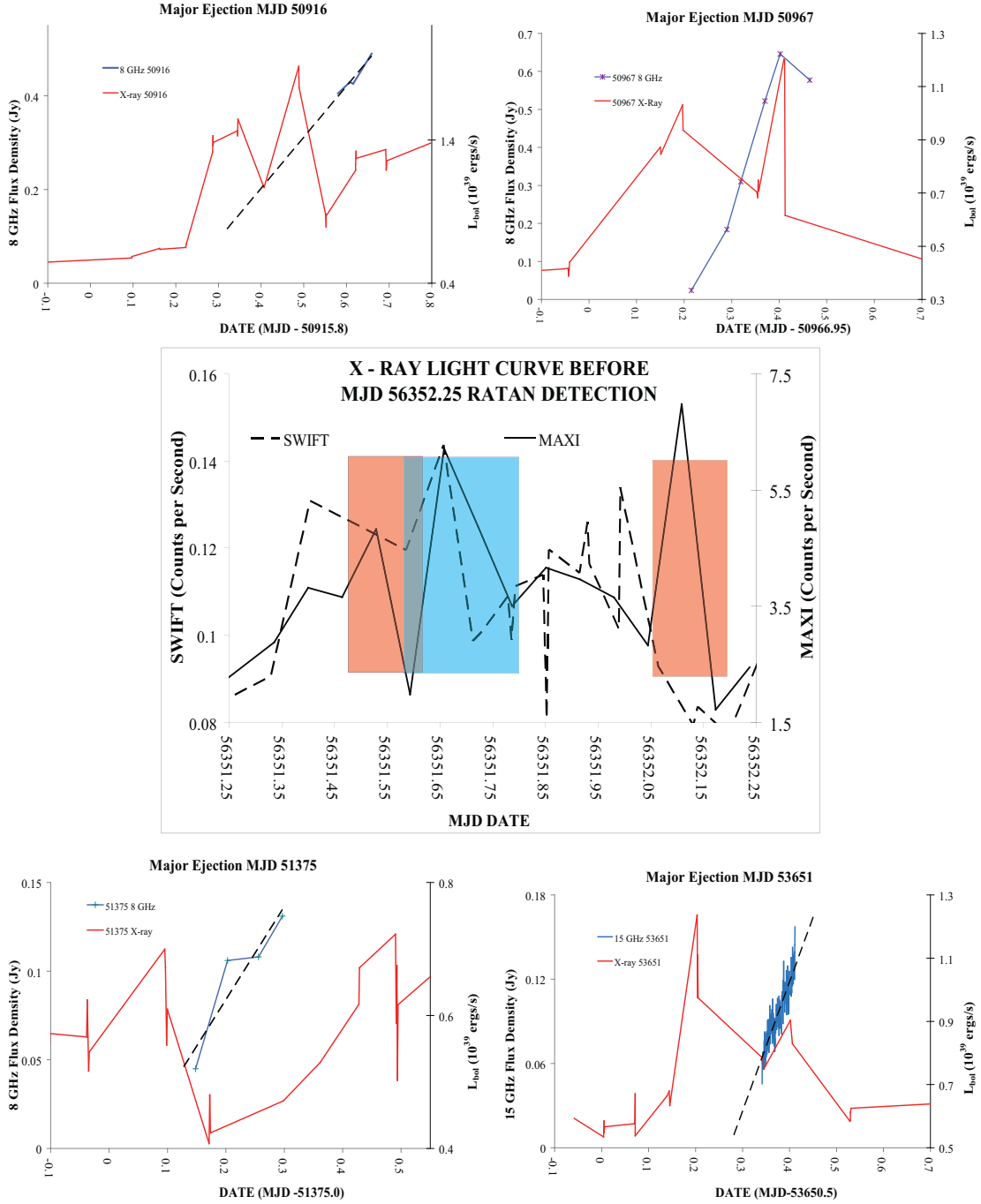


Fig. 1.— A montage comprised of previously published X-ray (RXTE/ASM) light curves associated with major flares in the four corners of the figure with the MAXI 2 keV - 20 keV and SWIFT/BAT 10 keV - 50 keV light curves before the 56352.245 radio flare plotted in the middle frame. The radio data (blue) and the associated trend line (dashed black) for the four historical light curves are plotted over the estimated interval of the MFE from PR13 and Punsly and Rodriguez (2013b). In the central frame, the shaded red (blue) area represents the minimal (maximal) ejection duration from the sample in PR13.

5. There can be large spikes in the light curve during the MFE which can exceed the X-ray luminosity before the launch. These spikes can occur during the ejection proper (see the MJD 50916 light curve in Figure 1) or immediately after the ejection episode has terminated (see the MJD 50967 light curve in Figure 1).
6. From the data in PR 13, the widest possible range of ejection episode durations for flares with 200 mJy to 400 mJy flux density at 4.8 GHz is 0.13 days to 0.20 days.

The other light curves associated with major flares in PR13 are consistent with the behaviors of the four light curves in Figure 1 that are listed above. However, there is insufficient data sampling during the launch proper to demonstrate more than points 1 and 6 above. Hence, we need to rely heavily on this small subsample. In general, the 6 items above should be sufficient to greatly restrict the plausible ejection epochs for individual flares from MAXI light curves that are typically sampled every 0.06 days.

### 3.1.2. *Prominent Features in the X-ray Light Curve*

We implement the 6 X-ray diagnostics of flare ejection to estimate the epoch of ejection corresponding to the Flare 2 in Table 1. This is actually a fairly complicated light curve. There are three spikes in the MAXI count rate between the flare non-detection by RATAN-600 on MJD 56351.248 (dropping the MJD, hereafter) and the detection on 56352.245: 56351.54, 56351.66 and 56352.13. The red (blue) shaded areas in Figure 1 correspond to the minimum (maximum) plausible ejection duration from point 6, 0.13 (0.20) days. We consider the prominent features of X-ray light curve in the context of the 6 points above:

- **Dip (56351.59):** The abrupt dip following a large spike in the X-ray light curve at 56351.59 is typical of X-ray light curves during ejection, never before ejection (see point 3 above). Thus, we conclude that the ejection begins before the dip and ends after the dip.
- **Spike 1 (56351.54):** Recall the pattern described by points 1 - 3 above: a large spike in the X-ray light curve precedes ejection and appears just before large fluctuations in the light curve that typically show a very large dip during the ejection episode. Spike 1 precedes the profound dip at 56351.59 and fits this pattern. We conclude that Spike 1 is either just before or during the ejection. The data and our method are insufficient to discriminate between the possibilities. Due to gaps in the MAXI coverage, one cannot assume that the actual local maximum of the light curve has been captured by the

observations. Formally, one can only restrict the actual light curve local maximum (Local Maximum 1):  $56351.47 < \text{Local Maximum 1} < 56351.58$ .

- **Spike 2 (56351.66):** Comparison to other light curves in Figure 1 indicates that Spike 2 is either during the ejection episode or immediately following ejection (point 5 above). Again, the data and our method are insufficient to discriminate between the possibilities. Due to temporal gaps in the MAXI coverage, as above, one can only restrict the associated local maximum in the light curve (Local Maximum 2) by  $56351.60 < \text{Local Maximum 2} < 56351.72$ .
- **Spike 3 (56352.13):** Spike 3 is only 0.11 days from the well developed flare observed by RATAN, this is too close in time to be probable from an evolutionary standpoint (PR13). Furthermore, the red shading shows that it is too brief to be responsible for jet launch since the MAXI counts are already low before 0.13 days have elapsed (point 6) and remain low up until the RATAN observation. By contrast, according to point 4, we expect a high average X-ray luminosity during the ejection. Finally, the suppressed SWIFT counts (from 10 keV - 50 keV) shows that the X-ray spectrum is very steep. This phenomenon of very luminous variable steep spectrum X-ray states *after* major ejections is well documented (Dhawan et al. 2000; Namiki et al. 2006; Trushkin et al. 2007). Thus, based on these three reasons, we conclude that Spike 3 is not associated with flare launch.

### 3.1.3. Ejection Episode Start Time

From the first and second bullets in subsection 3.1.2, we conclude that the ejection begins before the dip at 56351.59 and ends after the dip. Equivalently, the latest possible start date is 56351.58. From point 1 in subsection 3.1.1, we expect a large spike in the X-ray luminosity before the MFE. From bullet 2 in subsection 3.1.2 this occurs at  $56351.47 < \text{Local Maximum 1} < 56351.58$ . Thus, we conclude that the major ejection begins between 56351.47 and 56351.58.

### 3.1.4. Ejection Episode End Time

Applying the historical range of ejection durations from point 6 in subsection 3.1.1, of 0.13 days to 0.20 days to the range of start times in subsection 3.1.3 will bound the end of the MFE. In summary, we estimate that the major ejection begins between 56351.47 and 56351.58 and ends between 56351.60 and 56351.78.

### 3.2. Time Resolved Spectroscopy of Flare 2

Based on our estimates of the ejection episodes above, we use the MAXI spectral data to look for spectral evolution before and during ejection (i.e., we are looking for evidence of the physical mechanism responsible for ejection). Since the sensitivity of MAXI is low (low effective area), binning of the data over several times the temporal resolution is often required in order to constrain our spectral fits. This greatly reduces the time resolution except at strong peaks. The results obtained from the spectral fits with a model consisting of an absorbed powerlaw (`tbabs*powerlaw` in XSPEC terminology) with abundances obtained from Wilms et al. (2000) to the MAXI data from 1 keV to 20 keV are listed in Table 2. The first column represents the range of dates in each bin. The second column is the fitted column density of hydrogen,  $N_H$ , responsible for the effects of absorption in the spectrum. The third column is the photon index of the power law fit to the data,  $\Gamma$ . The next two columns are the absorbed flux and the unabsorbed (intrinsic) flux that de-convolves the effects of  $N_H$ . The last column is the reduced  $\chi^2$  figure of merit of the fit. The errors on the fitted parameters are at 90% confidence and the errors on the flux are at 68% confidence ( $1\sigma$ ). There are some evident trends in Table 2 for the 56352.245 flare. Obviously, the luminosity increases before the ejection. But, we also see  $\Gamma$  steepen and this steep spectrum seems to continue during the luminosity variations that occur during the ejection. The uncertainty in the photon index in Table 2 makes this phenomenon less than statistically significant. However, we also see an increase  $N_H$  with more statistical significance and we explore this below in Figure 2. The data in Figure 2 (from Table 2) is suggestive of a steady increase in  $N_H$  during the 15 hours preceding the ejection. However, the errors are large and it does not warrant such a strong statement without a statistical analysis. To this end note that the solid red line in Figure 2 is the fit to the data from 56350.85 up to 56351.54 using the method of least squares with uncertainty in both variables (Reed 1989). Equations (1) and (2) are the fits from 56350.85 up to dates 56351.54 and 56351.66, respectively:

$$N_H = (6.48 \pm 0.92)(\text{DATE} - 56350.65) + (5.27 \pm 0.57), \text{ DATE} \leq 56351.54, \quad (1)$$

$$N_H = (7.49 \pm 1.67)(\text{DATE} - 56350.65) + (4.83 \pm 1.20), \text{ DATE} \leq 56351.66. \quad (2)$$

The dashed lines in Figure 2 indicate the maximum and minimum slopes consistent with the data at the  $1\sigma$  level based on Equation (1). The slope and the corresponding uncertainty in Equation (1) indicates an increase in  $N_H$  at the  $\sim 6.5\sigma$  level preceding the flare.

Even though this result is statistically robust, we investigate if it is a manifestation of the degeneracy between  $\Gamma$  and  $N_H$  in the parametric spectral fits. Within a power law model, a modest low energy flux is only consistent with a large  $\Gamma$  if  $N_H$  is large as well. This is a consequence of the power law assumption. To this end, we use a nonparametric



Table 1: RATAN - 600 Radio Data Near Major Flare Ejections

Date MJD	Flux Density 4.8 GHz (mJy)	Flux Density 8.2 GHz (mJy)	Flux Density 11.2 GHz (mJy)
FLARE 1			
56312.349	$50 \pm 5$	$50 \pm 7$	$50 \pm 10$
56313	no observations		
56314.349	$364 \pm 18$	$243 \pm 24$	$234 \pm 23$
FLARE 2			
56349.253	$42 \pm 4$	no data	$51 \pm 8$
56350.250	$76 \pm 8$	no data	$76 \pm 6$
56351.248	$48 \pm 5$	no data	$80 \pm 8$
56352.245	$207 \pm 11$	$166 \pm 17$	$101 \pm 10$
56353.242	$100 \pm 10$	$100 \pm 10$	$100 \pm 10$

Table 2: Parametric Fits to MAXI Data Near Major Flare Ejections

Date MJD	$N_H$ $10^{22} \text{cm}^{-2}$	$\Gamma$	Observed Flux 1 - 10 keV $10^{-8} \text{ergs/sec-cm}^2$	Intrinsic Flux 1 - 10 keV $10^{-8} \text{ergs/sec-cm}^2$	Reduced $\chi^2(\text{dof})$
$56312.32 \pm 0.16$	$8.2^{+2.0}_{-1.7}$	$2.7 \pm 0.2$	$1.56 \pm 0.06$	$5.05 \pm 0.19$	1.40(79)
$56312.64 \pm 0.10$	$10.5^{+3.6}_{-3.0}$	$3.1^{+0.4}_{-0.3}$	$1.68 \pm 0.15$	$9.50 \pm 0.85$	1.20(42)
$56312.84 \pm 0.04$	$10.9^{+2.5}_{-2.1}$	$3.0 \pm 0.3$	$3.10 \pm 0.20$	$15.10 \pm 0.80$	0.90(66)
$56313.06 \pm 0.01$	$16.7^{+4.4}_{-3.5}$	$3.2^{+0.4}_{-0.3}$	$5.20 \pm 0.40$	$42.80 \pm 5.00$	1.35(41)
$56313.16 \pm 0.04$	$9.7^{+4.1}_{-3.1}$	$2.7^{+0.4}_{-0.3}$	$3.20 \pm 0.30$	$12.40 \pm 1.60$	0.90(27)
$56350.85 \pm 0.20$	$6.4^{+1.7}_{-1.4}$	$2.4 \pm 0.2$	$1.31 \pm 0.07$	$3.36 \pm 0.18$	0.88(75)
$56351.20 \pm 0.14$	$9.3^{+2.0}_{-1.7}$	$2.8 \pm 0.2$	$1.63 \pm 0.09$	$6.28 \pm 0.37$	1.27(68)
$56351.46 \pm 0.07$	$10.1^{+2.3}_{-2.0}$	$2.8 \pm 0.2$	$3.00 \pm 0.20$	$12.20 \pm 0.82$	0.90(62)
$56351.54 \pm 0.01$	$11.2^{+3.2}_{-2.7}$	$2.9 \pm 0.3$	$3.90 \pm 0.30$	$18.00 \pm 1.39$	0.80(43)
$56351.59 \pm 0.01$	$9.7^{+4.7}_{-3.4}$	$3.2^{+0.6}_{-0.5}$	$1.4 \pm 0.30$	$8.70 \pm 2.60$	0.90(19)
$56351.66 \pm 0.01$	$14.2^{+3.0}_{-2.5}$	$3.2 \pm 0.3$	$4.70 \pm 0.40$	$33.40 \pm 2.84$	1.00(55)
$56351.83 \pm 0.13$	$11.0^{+1.6}_{-1.4}$	$2.8^{+0.2}_{-0.1}$	$2.2 \pm 0.10$	$14.30 \pm 0.65$	0.99(117)

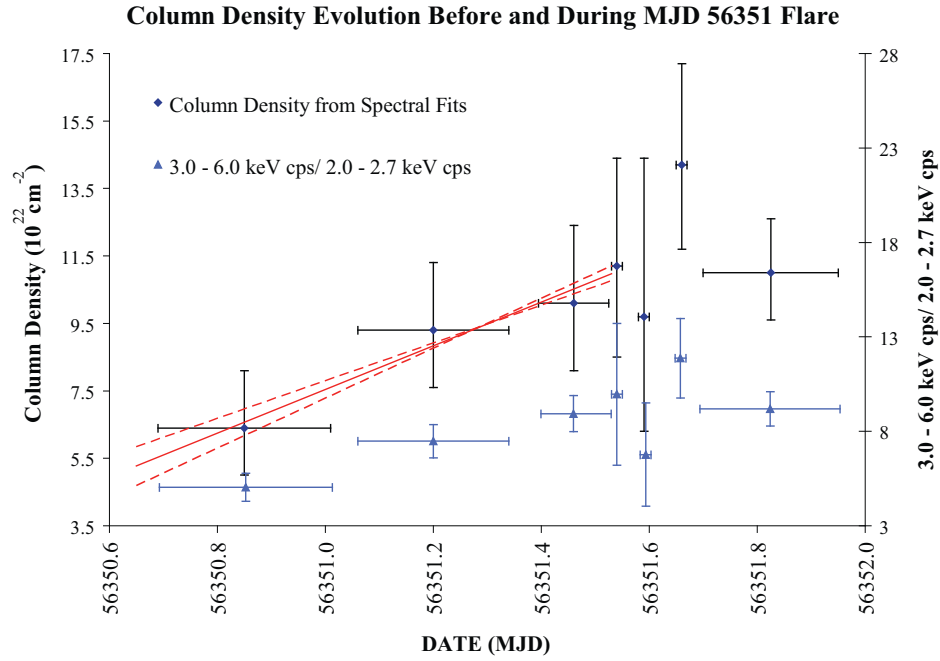


Fig. 2.— The fitted  $N_H$  from 56350.85 to 56351.83 from Table 2 is plotted in black. The fit to the data by the method of least squares with uncertainty in both variables from 56350.85 to 56351.54 is plotted as the solid red line. The maximum and minimum slopes associated with  $1\sigma$  uncertainty are the dashed red lines. The blue triangles are a nonparametric measure of absorption (the hardness in the soft band), the MAXI 3.0 keV - 6.0 keV cps divided by the 2.0 keV - 2.7 keV cps.

diagnostic, the ratio of counts per second (cps) in a MAXI bin from 3.0 keV to 6.0 keV (the spectral peak) to cps in the lowest MAXI energy bin 2.0 keV to 2.7 keV. Of course, the lowest energy bin is the most susceptible to the effects of absorption and the cps will be low and our statistics will suffer accordingly. Thus, considerable binning in the time domain is required to improve the statistics. The advantage of this nonparametric method of analysis is that it does not depend on  $\Gamma$  and the power law assumption. This removes the parametric degeneracy and replaces it with a ratio that is purely an empirical number. The blue data points indicate that the 2.0 keV to 2.7 keV cps are ever more suppressed relative to the 3.0 keV to 6.0 keV cps as the ejection is approached. This nonparametric analysis supports the power law based deduction that  $N_H$  increases before the major ejection.

### 3.3. MAXI observations of the Major Flare 1

Even though Flare 1 is larger than Flare 2, the MAXI data suffers from some inopportune gaps in temporal coverage and is inferior for our purposes. Figure 3 plots  $N_H$  from the spectral fits in Table 2, the MAXI 2 keV - 20 keV light curve and the SWIFT 10 keV - 50 keV light curve. The estimated range of possible ejection times, 56313.86 - 56314.06 are based on the 6 criteria listed above in Section 3. There was a large gap in MAXI coverage that envelopes most of the ejection episode. The statistics are poor because most of the luminous bins are lost due to the MAXI gap near ejection (when the fluxes were the highest). Furthermore, the X-ray cps decrease very rapidly after achieving a peak near 56314.0. Thus, large bins are required to get adequate statistics. The combination of wide ranges of dates in the bins and what appears to be a steep increase in  $N_H$  after 56313.8 results in an insufficient number of bins to resolve the increase. Thus, we cannot claim a large statistically significant increase in  $N_H$  preceding launch. The increase in  $N_H$  in Figure 3 before the MFE episode is consistent with the increase seen prior to the MFE that is responsible for Flare 2.

## 4. Conclusion

In this article, we examined time resolved MAXI X-ray spectroscopy of two major flares of GRS 1915+105 found with RATAN-600 radio monitoring during the first 8 months on 2013. The time resolved spectroscopy indicates that  $N_H$  increases as the X-ray luminosity increases before a major ejection and appears to remain elevated until the end of the ejection episode. This behavior was seen convincingly for Flare 2 and appears to be consistent with poorer data from Flare 1.

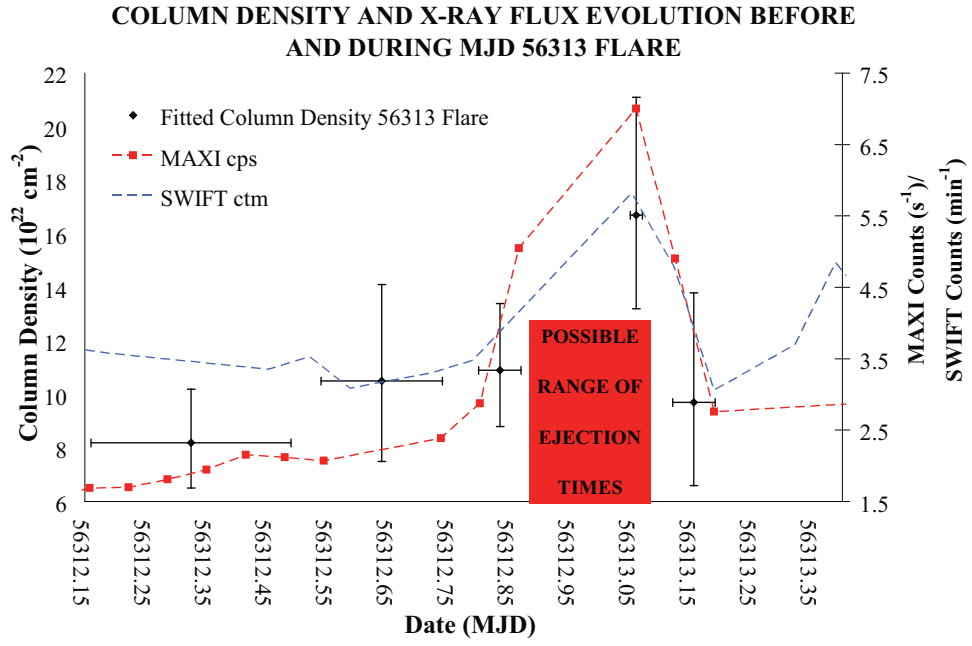


Fig. 3.— The MAXI light curve before Flare 1 is plotted in cps and the SWIFT light curve is plotted in ctm (counts per minute). The fitted column densities before the flare are taken from Table 2.

For the flares considered here, we determined that  $N_H$  increased by  $\approx 5 - 8 \times 10^{22} \text{cm}^{-2}$  over a time frame that begins a few hours before the initiation of the ejection and appears to extend well into the ejection episode. The increase of  $N_H$  can be cast in the light of the increase in the intrinsic absorption due to the column density located within the GRS1915+105 binary system,  $N_H(\text{intrinsic})$ . There is a significant component of the absorbing column due to the line of sight across the Galaxy, an extrinsic component,  $N_H(\text{extrinsic})$ . It was estimated in Chapuis and Corbel (2004) that  $N_H(\text{extrinsic}) \approx 3.5 \times 10^{22} \text{cm}^{-2}$ . The discussion in Belloni et al. (1997) indicates a slightly higher stable interstellar absorption column,  $N_H(\text{extrinsic}) \approx 4.5 \times 10^{22} \text{cm}^{-2}$ . From Table 2, this means that  $N_H(\text{intrinsic}) \approx 0.0 - 1.5 \times 10^{22} \text{cm}^{-2}$  12 - 15 hours before the ejection episode and increases by a factor  $> 10$  by the time of the ejection.

The increase in  $N_H$  has two obvious plausible physical interpretations

- The increase represents accreting gas at relatively high latitudes, since the line of sight is estimated at  $65^\circ - 70^\circ$  to the accretion disk normal from superluminal ejection kinematics (Mirabel and Rodriguez 1994; Fender et al. 1999). The additional high latitude accretion component is then a part of the triggering (and sustaining) mechanism of the major ejections.
- The enhanced absorbing column represents an out-flowing wind from the accretion disk that begins before a major ejection and continues during the ejection.

There is not enough data to conjecture deeply on these alternatives from a physical perspective. However, the first alternative is consistent with 3-D numerical simulations of accretion onto rotating black holes. A small class of simulations were found to be consistent with the correlation of the power of the ejection and the elevated X-ray luminosity. Namely, simulations that produced an ergospheric disk jet about a black hole with spin parameter  $a > 0.984$ . In the simulations, the jet power and the X-ray luminosity can be strong only during episodes of elevated accretion (Punsly and Rodriguez 2013c). In order to understand if the behavior of  $N_H$  seen here is endemic to large flares as opposed to anecdotal, we plan on continuing the RATAN monitoring to find more major flares. In particular, because of the correlation of radio luminosity before and during ejections and the X-ray flux found in PR13, stronger radio flares will have larger corresponding X-ray fluxes around the ejection episode. Thus, an extremely powerful flare (i.e., larger than 500 mJy at 4.8 GHz) will have large MAXI cps and smaller bins can be used thereby improving the time resolution and the statistics.

## 5. Appendix: Other Steep Spectrum Radio Flares in 2013

In this Appendix, we describe the other steep spectrum radio flares from the first 8 months of 2013 with  $> 100$  mJy flux density at 4.8 GHz,  $S_\nu(4.8 \text{ GHz}) > 100$  mJy. None of these flares have suitable X-ray data for time resolved spectroscopy.

- 56439.87 is the date of the RATAN-600 detection of the first of a series of flares that culminated in the large flare on 56352.25 (Flare 2) that was described at length in the text. RATAN-600 measured  $S_\nu(4.8 \text{ GHz}) \approx 140$  mJy and the spectrum was steep. Unfortunately, the MAXI scan stopped on GRS 1915+105, and did not complete when MAXI turned off its high voltage in order to protect X-ray detectors in a high radiation region. The process removed the data since the scan did not complete (Tatehiro private communication 2013).
- 56445.25 is the date of the RATAN-600 detection of  $S_\nu(4.8 \text{ GHz}) \approx 120$  mJy and the spectrum was steep. Unfortunately, MAXI did not cover GRS 1915 during the flare (Tatehiro private communication 2013).
- On 564543.97, RATAN-600 measured  $S_\nu(4.8 \text{ GHz}) = 175 \pm 15$  mJy and the spectrum was steep. The 2 keV - 20 keV MAXI light curve that was sampled every 0.06 days was in the range of 1.7 cps to 2.8 cps near the time of flare launch (the local maximum). This is less than half of what we found near the ejection period for Flare 2 in Figure 1 and about 1/3 of the count rate for Flare 1 in Figure 3 with the same bin size in the time domain. Thus, the count rate is too low for time resolved spectroscopy as the uncertainty in the fits would be enormous due to the low number statistics. This could be compensated for by approximately doubling the bin size in the time domain, but this would not provide meaningful time resolution. This modest flare highlights the importance of isolating the strongest radio flares for MAXI time resolved spectroscopy.
- The flare on 56487.87 detected by RATAN-600 was not formally steep:  $S_\nu(4.8 \text{ GHz}) = 163 \pm 16$  mJy,  $S_\nu(8.2 \text{ GHz}) = 160 \pm 16$  mJy and  $S_\nu(11.2 \text{ GHz}) = 107 \pm 11$  mJy. It is steep spectrum from 8.2 GHz to 11.2 GHz, but flat spectrum between 4.8 GHz and 8.2 GHz. It seems likely that  $S_\nu(4.8 \text{ GHz})$  would be larger than 100 mJy and steep spectrum a few hours later if the radio emitting plasma were in a state of rapid expansion. Unfortunately, like the 56439.87 radio flare, the MAXI scan stopped on GRS 1915+105, and did not complete. The process removed the data since the scan did not complete (Tatehiro private communication 2013).

This research has made use of MAXI data provided by RIKEN, JAXA and the MAXI team. BP would like to thank Tatehiro Mihara of the MAXI team for helping with the data acquisition and analysis. JR acknowledge funding support from the French Research National Agency: CHAOS project ANR-12-BS05-0009 (<http://www.chaos-project.fr>). JR also acknowledges financial support from the UnivEarthS Labex program of Sorbonne Paris Cit (ANR-10-LABX-0023 and ANR-11-IDEX-0005-02). SAT is thankful to Russian Foundation for Base Research for support (Grant N12-02-00812). We were also very fortunate to have a referee who offered many useful comments.

## REFERENCES

- Belloni, T. et al. 1997, ApJL 488 109
- Chapuis, C., Corbel, S. 2004, A & A 414 659
- Dhawan, V., Mirabel, I.F., Rodriguez, L. 2000, ApJ 343 373
- Done, C., Wardzinski, G., Gierlinski, M. 2004, MNRAS 349 393
- Fender, R. et al., 1999, MNRAS 304 865
- Fender, R., Belloni, T., Gallo, E. 2004, MNRAS 355 1105
- Matsuoka, M. et al., 2009, PASJ, 61, 999
- Miller-Jones, J. et al. 2005, MNRAS 363 867
- Miller-Jones, J. et al. 2012, MNRAS 421 468
- Mirabel, I.F., Rodriguez, L. 1994, Nature 371 46
- Muno, M., Morgan, E, Remillard, R. 1999, ApJ 527 321
- Namiki, M., Trushkin, S., Kotani, T., Kawai, N., Bursov, N., fabrika, S. 2006, VI Microquasars Workshop: Microquasars and Beyond, September 18-22, 2006, Societa del Casino, Como, Italy PoS(MQW96)083
- Novikov, I. and Thorne, K. 1973, in *Black Holes: Les Astres Occlus*, eds. C. de Witt and B. de Witt (Gordon and Breach, New York), 344
- PR13 Punsly, B., Rodriguez J. 2013a, ApJ 764 173
- Punsly, B., Rodriguez J. 2013b, ApJ 770 99

- Punsly, B., Rodriguez J. 2013, MNRAS 435 2322
- Reed, B. 1989, Am. J. Phys. 57 642
- Rodriguez, L., Mirabel, I.F. 1999, ApJ 511 398
- Rodriguez, J. et al. 2008, ApJ 675 1436
- Rushton, A., Spencer, E., Fender, R. and Pooley, G. 2010, A & A 524 29
- Trushkin, S. A.; Kotani, T.; Kawai, N.; Namiki, M.; Fabrika, S. N. Black Holes from Stars to Galaxies – Across the Range of Masses. Edited by V. Karas and G. Matt. Proceedings of IAU Symposium #238, held 21-25 August, 2006 in Prague, Czech Republic. Cambridge, UK: Cambridge University Press, 2007, 461
- Trushkin, S. A., Bursov, N.N., Nizhelskij N.A. 2008, AIP Conference Proceedings, 1053, 219.
- Wilms, J., Allen, A., McCray, R. 2000, ApJ 524 914